The absorption spectrum of guanine based radicals: a comparative computational analysis

Lara Martínez Fernández,[1] Javier Cerezo,[1] Haritha Asha,[2]
Fabrizio Santoro,[3] Sonia Coriani,[4] Roberto Improta[2,*]

May 6, 2019

[1]Departamento de Química, Facultad de Ciencias, Modúlo13 ,Universidad Autónoma de Madrid, Campus de Excelencia UAM-CSIC, Cantoblanco, 28049 Madrid, Spain,

[2]Istituto di Biostrutture e Bioimmagini-CNR, Via Mezzocannone 6,I-80134 Napoli,

[3]Istituto di Chimica dei Composti Organometallici (ICCOM-CNR), Area della Ricerca del CNR, Via Moruzzi 1, I-56124 Pisa,

[4]DTU Chemistry, Technical University of Denmark, Kemitorvet Building 207, DK-2800 Kongens Lyngby, Denmark

[*]e-mail:robimp@unina.it

Abstract

The excited states of the three radical derivatives of guanine, i.e. guanine cation (G^+) and its two main deprotonated derivatives (G-H1 and G-H2) have been characterized in the Franck-Condon region by TD-DFT, using different functionals, CASPT2, and EOM-EE-CCSD calculations. In the gas phase, all the methods provide a similar description of the main spectral features, the pictures provided by TD-DFT, with long range corrected functionals, and EOM-EE-CCSD being very close. Solvent effects are then taken into account by a mixed discrete-continuum approach, including five water molecules of the first solvation shell and the Polarizable Continuum Model (PCM). The vibronic absorption line-width has finally been simulated at the TD-M052X level by a time dependent method within the harmonic approximation. The resulting absorption spectra are in good agreement with their experimental counterparts, providing useful indications on the use of PCM/TD-DFT based approaches to interpret the spectra of guanine based radicals within DNA.

1 Introduction

Guanine exhibits the lowest ionization potential among the four DNA bases,[1, 2, 3] making its oxidation one of the most frequently occurring lesions in DNA.[4, 5, 6, 7, 8] Very recent experimental works have shown that absorption of a single low-energy UV photon at 265 nm can ionize guanine, with appreciable quantum yield ($> 10^{-3}$) in double strand DNA [9, 10] and quadruple helices (G-quads).[11, 12] Guanine cation (G^+) is also involved in the Electron Transfer (ET) and Proton Coupled Electron Transfer (PCET) processes that are caused in oligonucleotides by UV absorption,[13, 14, 15, 16, 17] and it is easily generated in the presence of oxidizing species.[4, 18, 19, 20, 21, 22, 23]

G^+ can trigger a cascade of photochemical events. Studies on the 'free' nucleotide in solution indicate that it is, indeed, unstable with respect to deprotonation and that the two most stable radicals species involve the loss of the proton bound to N1 (hereafter G-H1) or to the amino group (G-H2), see Figure 2.[24, 25, 26, 27] In water, G^+ is stable only for pH ≤ 3. For higher pH, it exists as G-H1 or, if the N1 proton is substituted by a methyl group, being deprotonation impossible, as G-H2.[24, 25]

The experimental absorption spectra of these three compounds are available (see Figure 1)[24, 26] and have been used as reference in order to identify the formation of G^+ in DNA and follow the kinetics of the subsequent reactions.[9, 11] On the other hand, the three spectra are rather similar, making a firm assignment of the time-resolved (TR) spectra in DNA very difficult, especially when considering that the spectral properties of the radical could be affected by its inclusion in the oligonucleotides and sensitive to conformational rearrangements of the strands. An accompanying computational analysis is useful, since it could give access to the spectra of the different radicals within the oligonucleotides and insights on the electronic/structural parameters affecting their optical properties. In fact, in some recent papers, the TR-spectra of G-derived radicals in guanine quadruplexes and in duplexes have been interpreted with the help of

Time Dependent Density Functional (TD-DFT) calculations, using M052X or CAM-B3LYP functionals.[9, 11, 12] The spectra computed in water for G^+, G-H1 and G-H2, including solvent effect by a mixed discrete continuum model (see Figure 2), are indeed in fair agreement with their experimental counterpart, supporting the reliability of this method to simulate the spectra within DNA, resorting to a mixed QM/MM approach.[9, 11, 12] On the other hand, as we will discuss below, there is still room for improvement of the accuracy of the spectra computed for G-based radicals, which, *inter alia*, have been simulated by simply convoluting the computed vertical transitions with a phenomenological gaussian, i.e. neglecting vibronic effects. This approach, though practical and cost-effective, could suffer from severe limitations when studying processes where the analysis of the absorption line-shapes is critical even for a qualitative assignment of the spectra. We thus decided to investigate in detail the absorption spectra of G^+, G-H1, and G-H2, in order to assess the reliability of TD-DFT calculations and the effects modulating their spectral properties. We shall compute in the gas phase the lowest energy excited states of the three radical derivatives of 9*H*-guanine by using Complete-Active-Space Second-Order Perturbation Theory (CASPT2), Equation-of-Motion Coupled Cluster Singles and Doubles (EOM-EE-CCSD) and TD-DFT calculations, testing the accuracy of eight different functionals.

The importance of vibronic effects in determining the absorption line-shape will then be assessed by simulating, with the harmonic approximation, the vibrationally resolved absorption spectra of the three radical species in the gas phase, by means of time-dependent methods implemented and profitably used by some of us [28, 29, 30] in the last few years on several classes of compounds.

Solvent effects will be added using the 9-Methylguanine as a model (to mimic the presence of the sugar) and a mixed continuum/discrete method, i.e. including five water molecules of the first solvation shell and the Polarizable Continuum Model (PCM).

Finally, the spectra of the three radicals in water will be critically compared with the available experimental spectra.

A full elucidation of the deprotonation dynamics of G^+ is an important step for what concerns not only our understanding of photoactivated dynamics of Nucleic Acids and, therefore, of the possible damage of the genetic code, but also for the use of DNA-based optolectronic materials.[31, 32]

Furthermore, from the methodological point of view, this study aims to provide useful reference data in the field of the excited state characterization of open-shell molecular species, where the number of comparative computational studies is still limited[33, 34, 35, 36, 37, 38] and the existence of many close-lying electronic transitions may render the vibronic calculations very challenging.

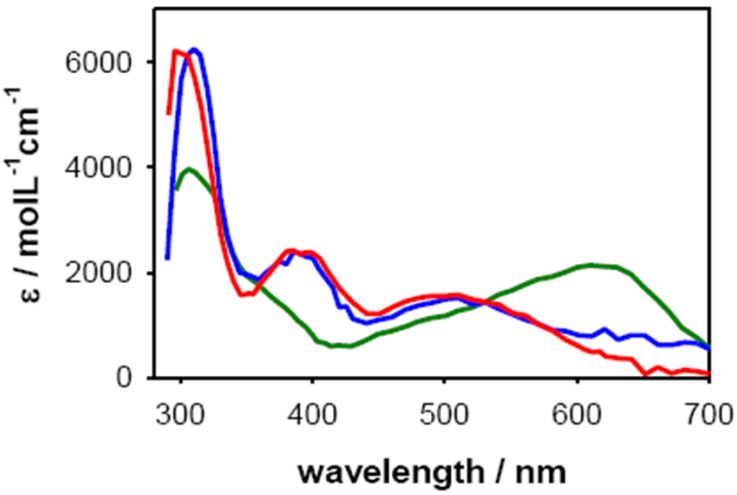

Figure 1: Experimental absorption spectra of monomeric guanine nucleotide radicals (GMP) in water solution. Radical cation $(G)^+$ (red), deprotonated (G-H1) radical (blue) and deprotonated (G-H2) radical (green). Elaboration of the spectra shown in ref.[24].

2 Computational Details

DFT calculations Ground state geometry optimizations have been performed at the

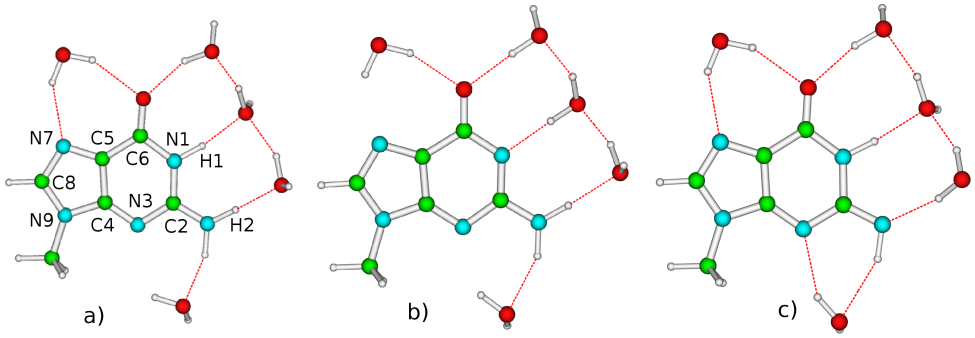

Figure 2: Schematic drawing of the computational models ($5H_2O$/PCM, including 5 explicit water molecules) used for the different systems in water; a) 9-Methylguanine, G (see atom labels), b) deprotonated (G-H1) radical, c) deprotonated (G-H2) radical. In 9*H*-guanine the methyl group at N9 is substituted by a H atom.

M052X/6-311G(d,p) level of theory, imposing C_s symmetry, for all the calculations not including explicit water molecules. M052X[39, 40] has been selected because it has been tailored to produce a fairly accurate description of stacking interactions and has previously been profitably used to study oligonucleotides[13, 41], including guanine-based quadruplexes[11, 12, 42, 43]. We have performed test calculations using the geometries optimized by M052X with a smaller basis set (6-31G(d)) or by CAM-B3LYP[44] or B3LYP[45, 46] functionals, checking that the computed spectra do not significantly depend on these details.

We studied the cationic form of the keto-amino tautomer shown in Figure 2, that has been shown to be the most stable in the gas phase[47]. Test PCM/M052X/6-311+G(d,p) calculations in water on $9-H$ guanine confirm that this tautomer is remarkably more stable than the enol and the imino tautomers, by 0.41 and 0.75 eV, respectively.

The 30 lowest energy excited states for each radical species have then been computed using TD-DFT, adopting, in addition to M052X, other long range corrected functionals, namely CAM-B3LYP[44], LC-BLYP[48], M062X[49], ωB97 and ωB97XD[50, 51].

These functionals have been shown to provide a fairly accurate description of the excited states in different amino acid radicals[36, 37]. The effect of the long range corrections on the computed spectra will be assessed by comparison with the results obtained by using two widely employed functionals as B3LYP and PBE0[52, 53], lacking those corrections. If not otherwise specified, we shall discuss the excited states obtained by using the 6-311+G(d,p) basis set. The effect of the size of the basis set has been tested by calculations employing the smaller 6-31G(d) and 6-31+G(d,p) basis sets.

CASPT2 calculations The absorption spectra of the different radicals were also modeled using CASPT2/CASSCF[54] calculations on top of the optimized M052X/6-31+G(d,p) minima in gas phase. An active space of 13 electrons in 11 orbitals was employed, consisting of 5 π and 4 π^*orbitals plus the lone pairs of the carbonyl group and the N7 atom, see Figures in the SI. The effect of including additional orbitals has been evaluated by using (15,13) larger active spaces. The 6-31G(d) basis set was used for these calculations, although the ANO-S[55] and ANO-L[56] basis set have been tested. The CASSCF state average calculations (SA-CASSCF) include 20 roots. An imaginary level shift[57] of 0.30 a.u was employed, whereas for the IPEA[58] shift two different values were considered, namely 0.0 and 0.25 au. Finally, the performance of both Single State (SS) and MultiState (MS) CASPT2 energies has been checked. These calculations have been carried out with OpenMolcas[59].

EOM-EE-CCSD calculations The stick spectra (energies and oscillator strengths) of the first eight excited states of the three radicals here considered were also computed using the EOM-EE-CCSD approach [60, 61] and the 6-311+G(d,p) basis set, at the optimized M052X/6-31+G(d,p) minima in gas phase. An unrestricted-Hartree Fock reference was adopted. The Qchem 5.2 [62, 63] program was used for the EOM-EE-CCSD calculations.

Solvation model Our analysis in solution has been performed on 9-Methylguanine, in order to enable a more direct comparison with the available experimental results.

We compare three approaches to model solvent effect. In the first one (PCM only), we simply resorted to PCM[64] implicit model to perform geometry optimizations and compute the spectra. Then, by using a mixed discrete-continuum approach[41, 65], we have optimized in water (treating bulk solvent effect by PCM) three molecular models including 5 water molecules of the first solvation shell (see Figure 2). The spectra have then been computed on the optimized structures both in the gas phase (5 H_2O/GP) and in water (5H_2O/PCM) allowing to discriminate on the different influence of solute/solvent hydrogen bonds and bulk effects on the spectra.

Vibronic calculations For each transition up to $D_0 \rightarrow D_8$ ($D_0 \rightarrow D_{12}$ in SI), the full line-shape arising from the vibrational structure has been simulated within the Born-Oppenheimer approximation. Namely, it is evaluated as the sum of the transitions between the vibrational levels in the adiabatic states, which can be recast as

$$\varepsilon(\omega) = \frac{4\pi^2 \omega N_A}{3 \times 1000 \times ln10 \times \hbar \times (4\pi\varepsilon_0)} \sum_{f=1}^{8} L_{g\rightarrow f}(\omega) \quad , \tag{1}$$

where symbols have the usual meaning (see e.g. ref. [66]) and the independent line-shapes for each transition, $L_{g\rightarrow f}(\omega)$, are evaluated through either a sum-over-states Time Independent (TI) formalism[66], or the Fourier Transform of the transition dipole correlation function, also known as Time Dependent (TD) formalism[67]. The TD approach is selected in this work as it provides fully converged line-shapes at any finite temperature by construction. The potential energy surfaces (PESs) for each state are described with harmonic expansions, which lead to analytic forms of the state-to-state vibronic intensities[68, 69] and correlation function[70, 71, 72, 73, 74], which appear in the TI and TD formalisms, respectively. Concretely, we adopt a vertical model in which all the PESs are expanded around the ground state minimum assuming constant transition dipole moments with respect to nuclear coordinates (Franck-Condon scheme). As a further approximation, the excited state (ES) Hessian is taken equal to the ground state (GS) one, while only the ES gradient is evaluated, which constitutes the Vertical Gradient (VG)[30] model. The vibronic calculations are conducted with

version 3.0 of the code *FCclasses*[75]. The vibronic transitions are broadened with a Gaussian convolution with Half Width at Half Maximum (HWHM) of 0.1 eV. Such additional broadening accounts for the effects not included in the model, namely, the inhomogeneous broadening due to the solvent[76], and it is adjusted to better fit the experiment.

The VG model avoids the computation of the ES Hessian and assumes a diabatic behaviour of the ES PESs, i.e., neglecting in practice any possible coupling among the states. However, the actual scenario can be significantly different as, in general, excited adiabatic states may be close enough to lead to conical intersections or avoided crossings. Analysis of the ES vibrational frequencies in the vertical (also known as Franck-Condon, FC) point can provide indications of the existence of these effects[77]. The frequency analysis at this non-stationary point is conducted using curvilinear internal coordinates[78], and indeed reveals a large coupling between the close excited states. In these circumstances, the spectral bands of the coupled states cannot be treated independently under the BO approximation, and inter-state couplings need to be explicitly taken into account. Recently, we approached such a situation to compute the non-adiabatic spectrum of cytosine in gas-phase, by multistate coupled quantum dynamics adopting a Linear Vibronic Coupling (LVC) model[79]. Although an analogous strategy could be adapted here to the cases when significant couplings are detected, this type of analysis would go beyond the scope of this work and we will only discuss the implications of neglecting the couplings.

3 Results

3.1 Gas Phase results

3.1.1 TD-DFT

A schematic description of the lowest energy excited states for the three guanine radicals under investigation is reported in Table 1 and in Figure 3. **In the following, we label as β the minority spin orbitals, and as α the majority spin, i.e. in the Ground**

State there is one additional α occupied orbital (HOMOα) with respect to β ones. HOMOα is very similar to the HOMO of the parent neutral G, whereas the similar β orbital is empty. Analogously, we label as HOMOβ the Highest Occupied β orbital in the GS. As could be expected, the lowest energy transitions involve β orbitals. M052X and CAM-B3LYP provide a very similar picture and in the following, whenever not specified, we shall refer to M052X results. For G^+, there are three bright transitions falling below 4 eV, with $\pi\pi^*$ characters (the MO's involved are depicted in Figure S1), which we will label as I^+, II^+, and III^+, in order of increasing energy and intensity. There are also three dark $n\pi^*$ transitions involving the transfer from the N and O Lone Pairs towards the LUMO β(Lβ). Finally, at $\sim$ 5 eV, we find the first electronic transition involving mainly α orbitals, a HOMOα $\rightarrow$LUMOα (Hα $\rightarrow$Lα) excitation (hereafter α^+ transition) similar to that responsible of the lowest energy absorption band in neutral G. In Table 1, only the dominant excitation is reported, but it is important to highlight that each transition receives contributions from multiple excitations. For example, H-1β $\rightarrow$Lβ excitation contributes to all the three lowest energy bright transitions, suggesting that the excited states could be significantly vibronically coupled.

According to our calculations, in the FC region the lowest energy excited states of G-H1 are qualitatively similar to those of G^+, with three bright excited states below 4 eV, whose intensity increases with the energy (hereafter transition I^{H1}, II^{H1} and III^{H1}) involving fairly similar MO's (see Figure S2), though some differences can be highlighted. For example, transition I^{H1} is more similar to II^+, and II^{H1} to I^+.

The computed spectrum of G-H2 is instead characterized by a low-energy bright transition at around 2.3 eV (I^{H2}), and it is less similar to those of G^+ and G-H1. G-H2 bears an imino substituent and, therefore, an exo-cyclic double bond; thus, it has different π orbitals (see Figure S3) and, consequently, rather different $\pi\pi^*$ transitions with respect to the two other radicals.

The computed spectra do not significantly change when adopting the smaller 6-

31G(d) basis set in the geometry optimization or in the excited state calculations (see Figure S4-S5).

The description of the FC region provided for the 3 radical species by the other long-range corrected functionals examined (shown in Figure S6) is similar to that of M052X and CAMB3LYP. The absorption line-shapes are similar, almost uniformly slightly red-shifted or blue-shifted with respect to the M052X spectra (see Table S1 and Figures S7-S9).

As a final step of our TD-DFT analysis in the gas phase, we have simulated the absorption spectra of 9-Methylguanine, in order to model with a Methyl substituent the effect of the sugar on the electronic properties of guanine radical species. The spectra (reported in Figure S10) are similar to those described above for 9H-guanine. Nonetheless, some differences are present: the most significant one involves the small red-shift ($\sim$0.2 eV) of I^{+} and II^{H1} (confirming their similar nature).

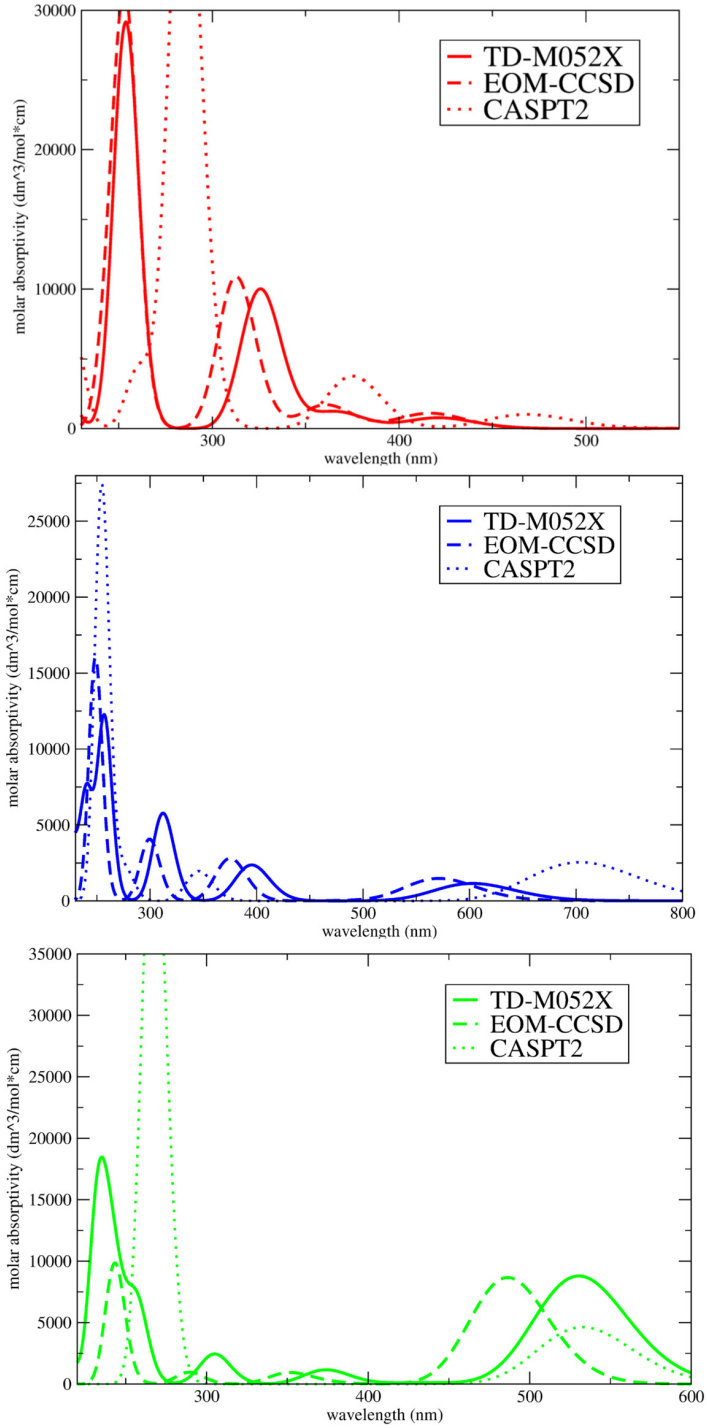

Figure 3: Spectra computed in the gas phase for 9*H*-guanine radicals. up) Radical cation G^+; central) deprotonated (G-H1) radical; bottom) deprotonated (G-H2) radical, by using different methods on the M052X/6-311G(d,p) optimized geometries. Continuous lines TD-M052X/6-311+G(d,p). Dashed lines EOM-EE-CCSD/6-311+G(d,p). Dotted lines SS-CASPT2/SA(20)-CASSCF(13,11)/6-31G(d). Each electronic transition is convoluted with a gaussian with HWHM=0.15 eV.

Table 1: 9H-guanine. Transition energies (ΔE, eV) and oscillator strengths (f, in parentheses, dimensionless, multiplied by 10^3) of the lowest energy electronic transitions at the (Franck-Condon) geometry for G^+, G-H1 and G-H2, according TD-M052X/6-311+G(d,p)//M052X/6-311G(d,p) calculations. The MO's involved in the dominant excitation for each transition are also shown.

Excited State	ΔE (f)	Excitation
	G^+	
D_1	2.10(0.1)	H$\beta \rightarrow$Lβ
D_2	2.63(0.0)	H-2$\beta \rightarrow$Lβ
D_3	2.94(8.6)	H-3$\beta \rightarrow$Lβ
D_4	3.37(13.3)	H-1$\beta \rightarrow$Lβ
D_5	3.80(111)	H-4$\beta \rightarrow$Lβ
D_6	3.88(0.1)	H-5$\beta \rightarrow$Lβ
D_7	4.87(255)	H$\alpha \rightarrow$Lα
D_8	4.93(77.1)	H$\alpha \rightarrow$L+1α
	G-H1	
D_1	1.41(0.1)	H-1$\beta \rightarrow$Lβ
D_2	2.05(12.7)	H$\beta \rightarrow$Lβ
D_3	2.27(0.2)	H-2$\beta \rightarrow$Lβ
D_4	3.13(26.3)	H-3$\beta \rightarrow$Lβ
D_5	3.38(0.0)	H-4$\beta \rightarrow$Lβ
D_6	3.97(64.2)	H-5$\beta \rightarrow$Lβ
D_7	4.39(0.2)	H-6$\beta \rightarrow$Lβ
D_8	4.82(134)	H$\alpha \rightarrow$L+1α
	G-H2	
D_1	2.33(97.7)	H$\beta \rightarrow$Lβ
D_2	2.45(0.0)	H-1$\beta \rightarrow$Lβ
		H-2$\beta \rightarrow$Lβ
D_3	2.85(1.3)	H-3$\beta \rightarrow$Lβ
D_4	3.17(0.0)	H-1$\beta \rightarrow$Lβ
		H-2$\beta \rightarrow$Lβ
D_5	3.31(12.9)	H-4$\beta \rightarrow$Lβ
D_6	4.06(27.2)	H-5$\beta \rightarrow$Lβ
D_7	4.35(0.1)	H-6$\beta \rightarrow$Lβ
D_8	4.83(76.3)	H$\alpha \rightarrow$Lα

3.1.2 EOM-EE-CCSD

As summarized in Table 2, EOM-EE-CCSD provides a description of the lowest energy excited states in the FC region consistent with the one yielded by M052X (and by the

other long-range corrected functionals). In detail, for G^+, all the bright excited states exhibit transition energies within ∼0.1 eV of the M052X ones, with similar intensity ratios. For G-H1, the EOM-EE-CCSD spectrum has a line-shape similar to the one of M052X, but for an almost uniform blue-shift of ∼0.15 eV. The EOM-EE-CCSD intensities are slightly larger, except for the transition III^{H1}. A small (∼0.2 eV), almost uniform, blue-shift with respect to M052X is predicted also for G-H2. In this latter case, the computed intensity of the lowest energy α transition is slightly larger than that of I^{H2}.

3.1.3 CASPT2

For what concerns G^+, SS-CASPT2 predicts, in agreement with M052X calculations, four bright states in the low energy region of the spectrum, which are red-shifted by ∼0.5 eV with respect to the M052X ones. The computed CASPT2 intensities are, on the average, larger than the M052X ones, though the pattern of the relative intensities of the different transitions is similar. For G-H1, as M052X, CASPT2 predicts four bright transitions below 5.5 eV. The lowest energy one is significantly red-shifted (and more intense) with respect to TD-M052X (by ∼0.4 eV), confirming the trends found for G^+. However, for G-H1, the other transitions are blue-shifted, and the intensity of the second and third peak is significantly smaller with respect to M052X, producing a spectrum rather different from the one obtained at the M052X (and EOM-EE-CCSD, see above) level.

For G-H2, CASPT2 and M052X are in good agreement, though the energy gap between I^{H2} and the bright α low energy transition is smaller according to the former method.

In order to verify the dependence of CASPT2 predictions on some relevant computational details, we have performed several test calculations on G-H1, the species showing the larger discrepancy with respect to not only TD-DFT and EOM-EE-CCSD calculations but also the experiments. As shown in Figure S14, neither the use of larger

basis set, the change on the IPEA shift, the inclusion of additional orbitals in the active space or the use of MS-CASPT2 qualitatively change the spectral patterns of G-H1.

Table 2: 9*H*-guanine. Transition energies (ΔE, eV) and oscillator strengths (f, in parentheses, dimensionless, multiplied by 10^3) of the lowest energy electronic transitions at the (Franck-Condon) geometry for G^+, G-H1 and G-H2, according to EOM-EE-CCSD/6-311+G(d,p) and SS-CASPT2/SA(20)-CASSCF(13,11)/6-31G(d) calculations. In the EOM-EE-CCSD results, the symmetry group of the transition is also reported.

Excited State	ΔE (f)	ΔE (f)
	EOM-EE-CCSD	SS-CASPT2
	G^+	
D_1	2.32(A" 0.191)	2.11(0.00)
D_2	2.84(A", 0.029)	2.46(0.00)
D_3	2.97(A', 12.2)	2.64 (11.3)
D_4	3.43(A', 19.0)	3.30 (41.9)
D_5	3.96(A', 121)	4.23 (31.2)
D_6	4.11(A", 0.208)	4.36 (482)
D_7	4.88(A', 317)	4.75(48.0)
D_8	5.06(A', 80.5)	5.47 (69.7)[a]
	G-H1	
D_1	1.66 (A", 0.167)	1.22(0.000)
D_2	2.16 (A', 16.4)	1.75 (26.6)
D_3	2.50 (A", 0.398)	1.79 (1.7)
D_4	3.30 (A', 31.2)	3.58(21.5)
D_5	3.56 (A", 0.000)	3.61 (0.3)
D_6	4.14 (A', 45.2)	4.47(22.4)
D_7	4.69 (A", 0.528)	4.80 (65.8)[b]
D_8	4.98 (A', 178)	4.88(248.9)[a]
	G-H2	
D_1	2.54 (A', 96.3)	2.32 (51.4)
D_2	2.88 (A", 0.132)	2.69 (2.6)
D_3	3.34 (A", 1.85)	2.94 (0.000)
D_4	3.53 (A', 9.48)	3.80 (1.9)
D_5	3.53 (A", 0.308)	3.92 (0.2)
D_6	4.28 (A', 10.7)	4.60 (280.4)
D_7	4.73 (A", 0.444)	4.67 (277.3)
D_8	5.09 (A', 109.6)	4.91 (9.7)

Notes: [a]corresponds to D_9, [b]corresponds to D_8

3.2 Absorption spectra in water

In Figure 4, we compare the spectra of the three radicals computed for the model $5H_2O$/PCM. The plots reported in Figure 4 have been obtained using a rather narrow gaussian in the convolution procedure, in order to better appreciate the position of the different transitions. Using larger values (see Figure S15), we indeed observe the merging of the peaks associated to transitions II^+ and III^+ and transitions I^{H1} and II^{H1}. As discussed below, this result is in better agreement with the indications of the vibronic calculations.

In order to assess the influence of hydrogen bonds and bulk solvent effects on each transition, we have computed the spectra of the three radical species in water, by using different solvation models. The spectra are reported in Figure S16-S18, where they are compared with those obtained in the gas phase. For G^+, transition I^+ is sensitive mainly to solute/solvent hydrogen bonds, whose inclusion slightly blue-shifts and increases the intensity of the corresponding electronic transition. Transition II^+ is significantly sensitive to both hydrogen bonds and bulk solvent effects: its intensity significantly increases with respect to the gas phase and the maximum red-shifts. As a consequence, while this transition in the gas phase appears as a small shoulder in the peak associated to III^+, in water it is much more prominent and gets closer to transition I^+. Transition III^+ is also red-shifted in water by solute/solvent hydrogen bonds, whereas the strong peak related to the 'α' transitions is not significantly affected by the solvent, but for a re-distribution of the intensity between the two corresponding electronic transitions induced by the water molecules. As a consequence, we have two close-lying peaks instead of one single band. On the other hand, it is clear that this picture is affected by the use of a single minimum for the cluster, while conformational averaging would probably lead to a single band.

For G-H1, transition I^{H1} is significantly blue-shifted by bulk solvation effects, while hydrogen bonds increase its intensity. The effect is opposite for transition II^{H2},

which is red-shifted with respect to the gas phase, leading to a partial merging of the two peaks. Bulk solvent effects influence mainly the intensity of transition III^{H1}, which increases, whereas α transitions are less affected by the solvent. For G-H2, the transition most sensitive to inclusion of solvent effect, especially to the bulk ones, is I^{H2}, which is red-shifted and becomes more intense when using the PCM.

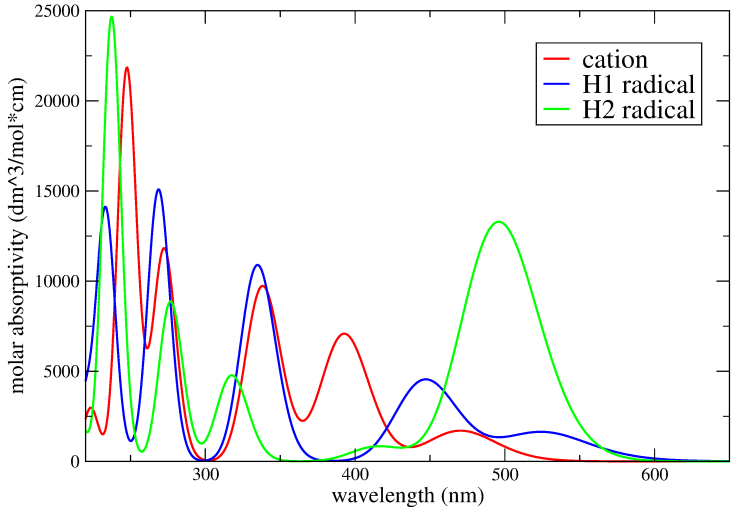

Figure 4: Computed absorption spectra of 9methyl guanine + 5 H_2O in water. Radical cation (G)+ (red), deprotonated (G-H1) radical (blue) and deprotonated (G-H2) radical (green). M052X/6-311+G(d,p)//M052X/6-311G(d,p) calculations. Each electronic transition is convoluted with a gaussian with HWHM=0.15 eV.

3.3 Vibronic spectra

The vibrationally resolved spectra computed for the three radical species using the procedure described above are reported in Figure 5. For G^+, I^+ and II^+ are responsible of the lowest energy absorption band (at $\sim$ 500 nm), III^+ of that at 400 nm, while the transitions involving α orbitals of the large absorption peak at $\sim$ 300 nm. The largest deviation with respect to the experimental spectra is the relative intensity of the 500 nm band. Keeping in mind the possible effect of non adiabatic couplings, this discrepancy is mainly due to the neglect of solvent effect, which, as discussed above, increases

the intensity of II^+. It is important to highlight that out calculations reproduce the absorption linewidth well. For example, the presence of two vibrational features at ∼380 nm and ∼400 nm is correctly predicted within the band at 400 nm.

For G-H1, according to our calculations the band at ∼ 500 nm is due to II^{H1}, that at 400 nm to III^{H1} and that at 300 nm to α^{H1}. I^{H1} contributes to the shallow red-wing tail. On the other hand, in water I^{H1} would blue-shift and become more intense. Inclusion of solvent effect would thus lead to an increase of the relative intensity of the 500 nm band, improving the agreement with the experimental results. Also for G-H1 the shape of the band at 400 nm is very well reproduced.

For G-H2, I^{H2} is responsible of the broad feature at 600 nm, whereas III^{H2} contributes to the high energy band at ∼ 300 nm, together with α transitions. II^{H2} is the responsible of the noticeable absorption between these to bands. Also for this molecule inclusion of solvent effect, which blue-shifts I^{H2}, is expected to further improve the agreement with the experimental results. Finally it noteworthy that when a larger number of excited states is considered in the calculation (see Figure S19) the relative intensity of the high-energy band at ∼ 300 nm significantly increases.

In general, our calculations provide an overall good prediction of the relative broadening of the different bands, correctly reproducing the large broadening of the lowest energy band in all cases. Our simulations also include an additional phenomenological broadening with a Gaussian convolution of HWHM=0.1 eV, which would account for the effect of the solvent. **The vibronic calculations are based on exactly the same electronic calculations as the phenomenological ones, so that we cannot expect a dramatic shift of the position of the peaks.** On the other hand, the comparison with the spectra obtained by mimicking the vibronic effects simply with a larger (0.25 eV) gaussian (shown in Figure 5) allows appreciating the importance of a proper inclusion of vibronic effects. For example, the phenomenological approach fails in reproducing the shape of the lowest energy band of G-H2 and in predicting non-zero absorption in the 400-500 nm range. Analogously, the shape of the band at ∼400 nm in G^+ and

G-H1 is correctly described only by vibronic calculations.

Compared with the experiment, however, some additional broadening effects seem to be missing; for instance, for G-H1, the high energy bands, well resolved in the simulation, are merged into a large band with a shoulder in the experiment. These differences can be explained by the neglected couplings between the states. Indeed, as we have already shown in a previous work describing the gas-phase spectra of cytosine, the coupling between the states would lead to an additional blurring of the bands[79]. Finally, it should be also be taken into account that in our calculations, we adopted the VG model, thus also neglecting the changes in the normal mode description upon the transition (Duschinsky effect) which would also lead to an additional broadening. VG approximation does not consider also the differences in the vibrational frequencies between ground and excited states. This limitation is expected to lead to a blue shift (0.1$\sim$0.2 eV)[29] of the computed spectra.

4 Concluding remarks

In this study, we report a thorough computational analysis of the absorption spectra of the guanine cation and the two species derived from its deprotonation. We analyze many of the factors affecting the shape of the computed spectra in water: (i) the chosen electronic structure method; (ii) the adopted computational model (9(H)-Gua vs. 9Methyl-Gua); (iii) the treatment of solvent effects; (iv) the inclusion of vibronic effects.

i) For what concerns the electronic structure method, TD-DFT calculations, for all the functionals examined, provide a very similar description of the excited states in the FC region and spectra reproducing the most prominent features of the experimental ones. Long-range corrections have a limited impact on the final picture and, actually, 'standard' hybrid functionals, as B3LYP and PBE0, are in better quantitative agreement with the experiments. On the other hand, these latter functionals cannot be used within DNA, due to their limitations in the description of Charge Transfer transitions. EOM-

EE-CCSD and TD-DFT spectra are rather similar, the former being uniformly slightly blue-shifted with respect to most of the functionals. CASPT2 calculations also provide a description of the excited states consistent with the experimental spectra. Most of the transitions are red-shifted with respect to the TD-M052X ones, so in better quantitative agreement with the corresponding experimental features. However, a conclusive assessment of the transition energy should be performed on the basis of the comparison of the whole spectral bands, also including vibronic effects, which is very computationally demanding at CASPT2 level. More significantly, CASPT2 does not reproduce the relative intensity of some transitions compared to the experiment, resulting in spectral lineshape different to the TD-DFT and EOM-EE-CCSD ones.

ii) Substitution in position 9 of an Hydrogen with a methyl group produces small but noticeable changes in the spectra, with a red-shift of the lowest energy bands of G^+ and G-H1, improving the agreement with the experiments. This is an important indication for QM/MM approaches, suggesting that the inclusion of the C1 atom of the sugar in the QM region, instead of limiting it to the bare purine rings, is desirable.

iii) Inclusion of solvent in the calculation also affects the spectra, for example increasing the relative intensity of the lowest energy transitions of G^+ and G-H1 (those responsible of the peak at $\sim$ 500 nm) and blue-shifting the I^{H1} and I^{H2} transitions. On balance, the spectra computed in water are in better agreement with their experimental counterpart, highlighting the necessity of a proper treatment of environmental effects. Both bulk effects and Hydrogen bonds influence the spectra, the relative importance of these two factors varying with the transition examined. This result represents another warning for the use of QM/MM approaches in the study of the radicals within DNA. It is possible that describing the inter-strand hydrogen bonds at the MM level is sufficient to catch their effect on the spectra. On the other hand, it is important to check whether non-polarizable Force Field can properly give account of the effect of the other bases (e.g. the stacked ones) on the excited states.

iv) The incorporation of vibronic effects represents one of the most significant re-

sults of this study. Our calculations allow to clearly identify the transitions responsible of the main absorption peaks, without relying exclusively on artificial inhomogeneous broadening. For example, it is clear that transitions I^+ and II^+ merge and are responsible of the lowest energy band in G^+. All in all, when solvent and vibronic effects are taken into account, the computed spectra are fully consistent with the experimental ones, reproducing their main features, but for a uniform blue-shift (see below). We find that for all the radicals a strong absorption band at $\sim$ 300 nm is present in the experimental spectra. Then, G^+ and G-H1 exhibit two bands at $\sim$ 400 and $\sim$ 500 nm, the latter being less intense and broader. We also correctly predict the existence of a broader red-tail for G-H1 and the very intense peak in the red-wing for G-H2.

Points (i)–(iv) made, some discrepancies still remain with the experimental spectra. In addition to the uniform blue-shift of the spectra (0.5$\sim$0.6 eV at the M052X and, presumably, CCSD levels), the absorption linewidth of the different bands is underestimated, i.e. the experimental spectrum is less resolved than the computed one. In general, our calculations overestimate the absorption intensity. Finally, the lowest energy band of G-H2 is too broad and too red-shifted (at least relatively to the other transitions) with respect to the experiments. Please note, however, that the computed intensity for this band is similar to that of the $\sim$ 400 nm peak of G-H1 and G^+, as in the experiments. The seeming overestimation of the intensity of the lowest energy band of G-H2 with respect to the band at 300 nm would indeed disappear when including a larger number of excited states in the spectrum, thus improving the description of the blue-wing of the spectrum (see Figure S19). Furthermore, it is important to remember that shifting all the transitions by the same value, though being useful for the comparison with the experimental spectrum, does not have any solid theoretical basis. In this respect, the seeming underestimation of the transition energy of I^{H2} could simply depend on the use of a too large shift.

Some of these discrepancies can be traced back to the effects that are not (yet) included in the treatment. The use of VG model gives account of a non negligible

part of the uniform blue-shift of the computed spectra with respect to experiments. As discussed above, Duschinsky effects and the non-adiabatic couplings between the excited states are not considered, leading to underestimate the absorption linewidth of the different bands.

At the moment, it is not possible, and it falls outside the scope of the present study, to predict the effect on the spectra of the other approximations of our treatment: the absence of sugar (mimicked by a simple methyl group), the neglect of the conformational fluctuations of the radical and in the solvation shell, and the use of a continuum model to treat the outer solvent shells.

Other features seem to depend on the reference electronic method, i.e. TD-M052X. It overestimates the intensity of the bright states, confirming previous indications[29], and the computed transition energies are blue-shifted with respect to those predicted by other functionals, as CAM-B3LYP or ωB97XD, which would likely provide spectra closer to the experimental ones.

These considerations confirm that the study of the optical spectra of open shell species is very challenging. Also when the multiplicity of the ground state is well assessed and in the absence of severe spin contamination in the computed excited states (and both conditions cannot always be taken for granted), many of the problems involved in the calculations of electronic spectra are more acute for radicals. We are often in the presence of many close-lying low-energy transitions, sometimes quite weak. Small errors in the transition energy and in the computed intensity can give rise to qualitatively wrong line-shapes, sometimes undermining the possibility of using calculations even for a qualitative assignment of the spectra. In this respect, a correct reproduction of the relative intensities of the different transitions, a feature often overlooked with respect to the accuracy in the prediction of the transition energies, is particularly important. As a matter of fact, the absorption intensity is often more informative on the nature of the radical than the absolute position of the bands, frequently shifted by a few nanometers only. Our results also suggest that the inclusion of non-adiabatic couplings

among the different states, which can significantly modify the absorption line-shape, is also more critical for open shell species.

For what concerns the perspectives on the use of QM calculations to assign the time-resolved spectra of G-based radical in DNA, our study provides multifaceted indications. On the one hand, when using long range corrected functionals, PCM/TD-DFT calculations are able to capture the most relevant spectral features of G^+, G-H1 and G-H2, providing, when vibronic effects are included, spectra in good agreement with the experiments. On this ground they can be profitably used to identify the most prominent features of the TR spectra. On the other hand, there are still discrepancies for what concerns the relative position ($0.1\sim0.2$ eV) and the intensity of the different bands. These errors are not large but, since the spectra of the radicals are very similar, they are of the same order of magnitudes of the most subtle spectral shifts recorded in the TR experiments. It is surely possible to further reduce the errors of our computational treatment but, at the same time, inclusion of the radical within DNA provides additional challenges to calculations and, consequently, additional sources of errors. On balance, we think that it is not yet possible to rely *only* on the analysis of the electronic spectra to fully elucidate the dynamical processes involving guanine based radicals in DNA, making desirable the integration of different techniques (Transient electronic and IR spectra, EPR spectroscopy) with their computational counterpart.

Acknowledgments

This work has received funding from the European Union's Horizon 2020 research and innovation programme MSCA-ITN under grant agreement No. 765266 (LightDyNAmics). RI thanks Dr. J. Green (IBB-CNR) for useful suggestions. SC acknowledges support from the Independent Research Fund Denmark – DFF-Forskningsprojekt2, grant no. 7014-00258B. Computational time from the Centro de Computación Científica (CCC) of Universidad Autónoma de Madrid is also gratefully acknowledged.

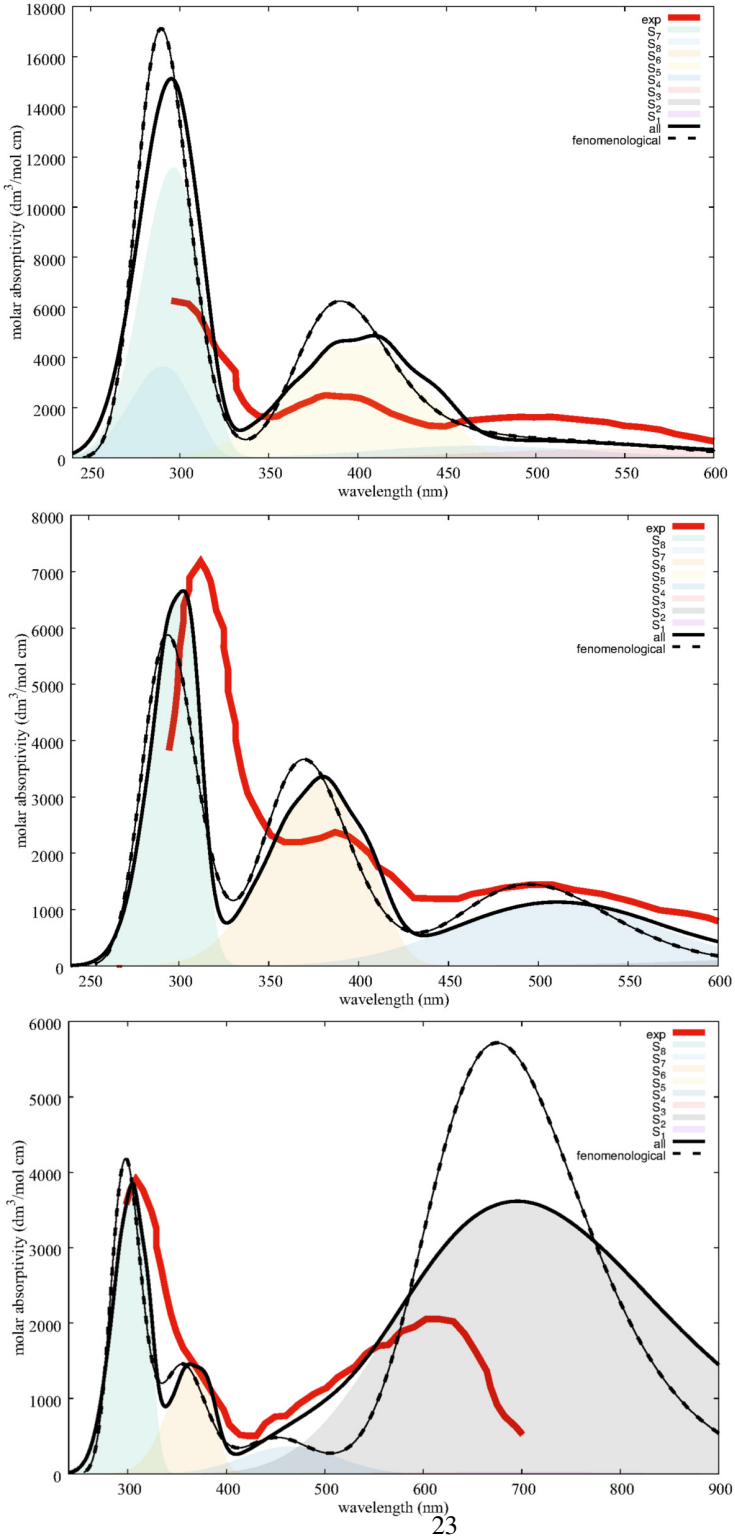

Figure 5: Computed vibrationally resolved absorption spectra in the gas phase for 9(H)-G radicals. up) Radical cation G^+; central) deprotonated (G-H1) radical; bottom) deprotonated (G-H2) radical. M052X/6-31G(d) calculations. Each vibronic transition is convoluted with a gaussian with HWHM=0.1 eV. The spectra obtained by simple convolution of the vertical transitions with a Gaussian of HWHM=0.25 eV are also shown. All the computed spectra are shifted by -0.6 eV. Experimental spectra from Ref. 2 are also shown.

References

[1] E. Paleček and M. Bartošík, *Chemical Reviews*, 2012, **112**, 3427–3481.

[2] S. Steenken and S. V. Jovanovic, *Journal of the American Chemical Society*, 1997, **119**, 617–618.

[3] C. E. Crespo-Hernandez, D. M. Close, L. Gorb and J. Leszczynski, *The Journal of Physical Chemistry B*, 2007, **111**, 5386–5395.

[4] J. Cadet, K. J. Davies, M. H. Medeiros, P. D. Mascio and J. R. Wagner, *Free Radical Biology and Medicine*, 2017, **107**, 13 – 34.

[5] E. Fouquerel, J. Lormand, A. Bose, H. T. Lee, G. S. Kim, J. F. Li, R. W. Sobol, B. D. Freudenthal, S. Myong and P. L. Opresko, *Nat. Struct. Mol. Biol.*, 2016, **23**, 1092.

[6] M. Gomez-Mendoza, A. Banyasz, T. Douki, D. Markovitsi and J. L. Ravanat, *J. Phys. Chem. Lett.*, 2016, **7**, 3945.

[7] S. Kanvah, J. Joseph, G. B. Schuster, R. N. Barnett, C. L. Cleveland and U. Landman, *Accounts of Chemical Research*, 2010, **43**, 280–287.

[8] J. Cadet and T. Douki, *Journal of Investigative Dermatology*, 2011, **131**, 1005 – 1007.

[9] A. Banyasz, L. Martínez-Fernández, R. Improta, T.-M. Ketola, C. Balty and D. Markovitsi, *Phys. Chem. Chem. Phys.*, 2018, **20**, 21381–21389.

[10] A. Banyasz, T. Ketola, L. Martínez-Fernández, R. Improta and D. Markovitsi, *Faraday Discuss.*, 2018, **207**, 181–197.

[11] A. Banyasz, L. Martínez-Fernández, C. Balty, M. Perron, T. Douki, R. Improta and D. Markovitsi, *J. Am. Chem. Soc.*, 2017, **139**, 10561–10568.

[12] L. Martínez-Fernández, A. Banyasz, D. Markovitsi and R. Improta, *Chem. Eur. J.*, 2018, **24**, 15185.

[13] R. Improta, F. Santoro and L. Blancafort, *Chem. Rev.*, 2016, **116**, 3540.

[14] K. Röttger, H. J. B. Marroux, M. P. Grubb, P. M. Coulter, H. Böhnke, A. S. Henderson, M. C. Galan, F. Temps, A. J. Orr-Ewing and G. M. Roberts, *Angewandte Chemie International Edition*, 2015, **54**, 14719–14722.

[15] Y. Zhang, K. de La Harpe, A. A. Beckstead, R. Improta and B. Kohler, *J. Am. Chem. Soc.*, 2015, **137**, 7059.

[16] Y. Zhang, K. de La Harpe, A. A. Beckstead, L. Martínez-Fernández, R. Improta and B. Kohler, *The Journal of Physical Chemistry Letters*, 2016, **7**, 950–954.

[17] L. Martinez-Fernandez and R. Improta, *Faraday Discuss.*, 2018, **207**, 199–216.

[18] J. P. Hall, F. E. Poynton, P. M. Keane, S. P. Gurung, J. A. Brazier, D. J. Cardin, G. Winter, T. Gunnlaugsson, I. V. Sazanovich, M. Towrie, C. J. Cardin, K. J. M. and S. J. Quinn, *Nature Chemistry*, 2015, **7**, 961–967.

[19] L. D. Wu, K. H. Liu, J. L. Jie, D. Song and H. M. Su, *J. Am. Chem. Soc.*, 2015, **137**, 259.

[20] J. Choi, J. Park, A. Tanaka, M. J. Park, Y. J. Jang, M. Fujitsuka, S. K. Kim and T. Majima, *Angew. Chem., Int. Ed.*, 2013, **52**, 1134.

[21] A. M. Fleming and C. J. Burrows, *Chem. Res. Toxicol.*, 2013, **26**, 593.

[22] Y. Rokhlenko, J. Cadet, N. E. Geacintov and V. Shafirovich, *J. Am. Chem. Soc.*, 2014, **136**, 5956.

[23] P. Di Mascio, G. R. Martinez, S. Miyamoto, G. E. Ronsein, M. H. G. Medeiros and J. Cadet, *Chemical Reviews*, 2019, **119**, 2043–2086.

[24] L. P. Candeias and S. Steenken, *J. Am. Chem. Soc.*, 1989, **111**, 1094.

[25] L. P. Candeias and S. Steenken, *J. Am. Chem. Soc.*, 1992, **114**, 699.

[26] C. Chatgilialoglu, C. Caminal, M. Guerra and Q. G. Mulazzani, *Angew. Chem., Int. Ed.*, 2005, **44**, 6030.

[27] C. Chatgilialoglu, C. Caminal, A. Altieri, G. C. Vougioukalakis, Q. G. Mulazzani, T. Gimisis and M. Guerra, *J. Am. Chem. Soc.*, 2006, **128**, 13796.

[28] F. J. Avila Ferrer, J. Cerezo, J. Soto, R. Improta and F. Santoro, *Comput. Theoret. Chem.*, 2014, **1040–1041**, 328–337.

[29] F. J. Avila Ferrer, J. Cerezo, E. Stendardo, R. Improta and F. Santoro, *J. Chem. Theory Comput.*, 2013, **9**, 2072–2082.

[30] F. J. Avila Ferrer and F. Santoro, *Phys. Chem. Chem. Phys.*, 2012, **14**, 13549–13563.

[31] J. C. Genereux and J. K. Barton, *Chem. Rev.*, 2010, **110**, 1642–1662.

[32] G. B. Schuster, *Accounts of Chemical Research*, 2000, **33**, 253–260.

[33] D. Roca-Sanjuán, M. Rubio, M. Merchán and L. Serrano-Andrés, *J. Chem. Phys.*, 2006, **125**, 084302.

[34] D. Roca-Sanjuán, M. Merchán, L. Serrano-Andrés and M. Rubio, *J. Chem. Phys.*, 2008, **129**, 095104.

[35] J. Segarra-Martí, M. Merchán and D. Roca-Sanjuán, *The Journal of Chemical Physics*, 2012, **136**, 244306.

[36] V. Riffet, D. Jacquemin, E. Cauët and G. Frison, *Journal of Chemical Theory and Computation*, 2014, **10**, 3308–3318.

[37] F. Tureček, *J. Phys. Chem. A*, 2015, **119**, 10101–10111.

[38] J. Segarra-Martí, T. Tran and M. J. Bearpark, *Phys. Chem. Chem. Phys.*, 2019, doi:10.1039/C8CP07189F.

[39] Y. Zhao, N. E. Schultz and D. G. Truhlar, *J. Chem. Theory Comput.*, 2006, **2**, 364.

[40] Y. Zhao and D. G. Truhlar, *Acc. Chem. Res.*, 2008, **41**, 157.

[41] R. Improta and V. Barone, *Top. Curr. Chem.*, 2014, **355**, 329.

[42] R. Improta, *Chem. - Eur. J.*, 2014, **20**, 8106.

[43] M. Deiana, B. Mettra, L. Martinez-Fernandez, L. M. Mazur, K. Pawlik, C. Andraud, M. Samoc, R. Improta, C. Monnereau and K. Matczyszyn, *J. Phys. Chem. Lett.*, 2017, **8**, 5915–5920.

[44] T. Yanai, D. Tew and N. Handy, *Chem. Phys. Lett.*, 2004, **393**, 51.

[45] A. D. Becke, *Phys. Rev. A*, 1988, **38**, 3098.

[46] C. Lee, W. Yang and R. G. Parr, *Phys. Rev. B*, 1988, **37**, 785.

[47] P. Cheng, Y. Li, S. Li, M. Zhang and Z. Zhou, *Phys. Chem. Chem. Phys.*, 2010, **12**, 4667–4677.

[48] H. Likura, T. Tsuneda, T. Yanai and K. Hirao, *J. Chem. Phys.*, 2001, **115**, 3540.

[49] Y. Zhao and D. G. Truhlar, *Theor. Chem. Acc.*, 2008, **120**, 215.

[50] J. D. Chai and M. Head-Gordon, *J. Chem. Phys.*, 2008, **128**, 084106/1.

[51] J. D. Chai and M. Head-Gordon, *Phys. Chem. Chem. Phys.*, 2008, **10**, 6615.

[52] C. Adamo and V. Barone, *J. Chem. Phys.*, 1999, **110**, 6158.

[53] M. Enzerhof and G. E. Scuseria, *J. Chem. Phys.*, 1999, **110**, 5029.

[54] B. Roos, in *in Ab initio Methods in Quantum Chemistry II. Lawley, K. P. Ed.*, Wiley, Chichester, 1987.

[55] K. Pierloot, B. Dumez, P. O. Widmark and R. B. O., *Theor. Chim. Acta*, 1995, **90**, 87.

[56] P. O. Widmark, P. A. Malmqvist and R. B. O., *Theor. Chim. Acta*, 1990, **77**, 291.

[57] N. Forsberg and P. A. Malmqvist, *Chem. Phys. Lett*, 1997, **274**, 196.

[58] G. Ghigo, B. O. Roos and P. A. Malmqvist, *Chem. Phys. Lett.*, 2004, **396**, 142.

[59] F. Aquilante, J. Autschbach, R. K. Carlson, L. F. Chibotaru, M. G. Delcey, L. De Vico, I. Fdez. Galván, N. Ferré, L. M. Frutos, L. Gagliardi, M. Garavelli, A. Giussani, C. E. Hoyer, G. Li Manni, H. Lischka, D. Ma, P. A. Malmqvist, T. Müller, A. Nenov, M. Olivucci, T. B. Pedersen, D. Peng, F. Plasser, B. Pritchard, M. Reiher, I. Rivalta, I. Schapiro, J. Segarra-Martí, M. Stenrup, D. G. Truhlar, L. Ungur, A. Valentini, S. Vancoillie, V. Veryazov, V. P. Vysotskiy, O. Weingart, F. Zapata and R. Lindh, *J. Comput. Chem.*, 2016, **37**, 506.

[60] A. I. Krylov, *Annual Review of Physical Chemistry*, 2008, **59**, 433–462.

[61] A. I. Krylov, *Reviews in Comp. Chem.*, J. Wiley & Sons, 2017, vol. 30, ch. 4, pp. 151–224.

[62] Y. Shao, Z. Gan, E. Epifanovsky, A. T. Gilbert, M. Wormit, J. Kussmann, A. W. Lange, A. Behn, J. Deng, X. Feng, D. Ghosh, M. Goldey, P. R. Horn, L. D. Jacobson, I. Kaliman, R. Z. Khaliullin, T. Kuś, A. Landau, J. Liu, E. I. Proynov, Y. M. Rhee, R. M. Richard, M. A. Rohrdanz, R. P. Steele, E. J. Sundstrom, H. L. W. III, P. M. Zimmerman, D. Zuev, B. Albrecht, E. Alguire, B. Austin, G. J. O. Beran, Y. A. Bernard, E. Berquist, K. Brandhorst, K. B. Bravaya, S. T. Brown, D. Casanova, C.-M. Chang, Y. Chen, S. H. Chien, K. D. Closser, D. L. Crittenden, M. Diedenhofen, R. A. D. Jr., H. Do, A. D. Dutoi, R. G. Edgar, S. Fatehi, L. Fusti-Molnar, A. Ghysels, A. Golubeva-Zadorozhnaya, J. Gomes, M. W. Hanson-Heine, P. H. Harbach, A. W. Hauser, E. G. Hohenstein, Z. C.

Holden, T.-C. Jagau, H. Ji, B. Kaduk, K. Khistyaev, J. Kim, J. Kim, R. A. King, P. Klunzinger, D. Kosenkov, T. Kowalczyk, C. M. Krauter, K. U. Lao, A. D. Laurent, K. V. Lawler, S. V. Levchenko, C. Y. Lin, F. Liu, E. Livshits, R. C. Lochan, A. Luenser, P. Manohar, S. F. Manzer, S.-P. Mao, N. Mardirossian, A. V. Marenich, S. A. Maurer, N. J. Mayhall, E. Neuscamman, C. M. Oana, R. Olivares-Amaya, D. P. O'Neill, J. A. Parkhill, T. M. Perrine, R. Peverati, A. Prociuk, D. R. Rehn, E. Rosta, N. J. Russ, S. M. Sharada, S. Sharma, D. W. Small, A. Sodt, T. Stein, D. Stück, Y.-C. Su, A. J. Thom, T. Tsuchimochi, V. Vanovschi, L. Vogt, O. Vydrov, T. Wang, M. A. Watson, J. Wenzel, A. White, C. F. Williams, J. Yang, S. Yeganeh, S. R. Yost, Z.-Q. You, I. Y. Zhang, X. Zhang, Y. Zhao, B. R. Brooks, G. K. Chan, D. M. Chipman, C. J. Cramer, W. A. G. III, M. S. Gordon, W. J. Hehre, A. Klamt, H. F. S. III, M. W. Schmidt, C. D. Sherrill, D. G. Truhlar, A. Warshel, X. Xu, A. Aspuru-Guzik, R. Baer, A. T. Bell, N. A. Besley, J.-D. Chai, A. Dreuw, B. D. Dunietz, T. R. Furlani, S. R. Gwaltney, C.-P. Hsu, Y. Jung, J. Kong, D. S. Lambrecht, W. Liang, C. Ochsenfeld, V. A. Rassolov, L. V. Slipchenko, J. E. Subotnik, T. V. Voorhis, J. M. Herbert, A. I. Krylov, P. M. Gill and M. Head-Gordon, *Mol. Phys.*, 2015, **113**, 184–215.

[63] A. I. Krylov and P. M. W. Gill, *WIREs Comput. Mol. Sci.*, 2013, **3**, 317–326.

[64] J. Tomasi, B. Mennucci and R. Cammi, *Chem. Rev.*, 2005, **105**, 2999.

[65] R. Improta, in *UV–visible absorption and emission energies in condensed phase by PCM/TD-DFT methods*, ed. V. Barone, Wiley, Chichester, 2012, ch. 1, pp. 39–76.

[66] M. Biczysko, J. Bloino, F. Santoro and V. Barone, in *Time-Independent Approaches to Simulate Electronic Spectra Lineshapes: From Small Molecules to Macrosystems*, ed. V. Barone, John Wiley & Sons, Inc., 2011, ch. 8, pp. 361–443.

[67] A. Lami and F. Santoro, in *Time-Dependent Approaches to Calculation of Steady-*

State Vibronic Spectra: From Fully Quantum to Classical Approaches, ed. V. Barone, John Wiley & Sons, Inc., 2011, ch. 10, pp. 475–516.

[68] T. E. Sharp and H. M. Rosenstock, *J. Chem. Phys.*, 1964, **41**, 3453–3463.

[69] A. Peluso, F. Santoro and G. Del Re, *Int. J. Quantum Chem.*, 1997, **63**, 233–244.

[70] J. Tang, M. T. Lee and S. H. Lin, *J. Chem. Phys.*, 2003, **119**, 7188–7196.

[71] R. Ianconescu and E. Pollak, *J. Phys. Chem. A*, 2004, **108**, 7778–7784.

[72] Q. Peng, Y. Niu, C. Deng and Z. Shuai, *Chem. Phys.*, 2010, **370**, 215–222.

[73] R. Borrelli, A. Capobianco and A. Peluso, *J. Phys. Chem. A*, 2012, **116**, 9934–9940.

[74] A. Baiardi, J. Bloino and V. Barone, *J. Chem. Theory Comput.*, 2013, **9**, 4097–4115.

[75] F. Santoro and J. Cerezo, *$\mathscr{FC}$classes3, a code for vibronic calculations. Available upon request*, 2019.

[76] F. J. Avila Ferrer, R. Improta, F. Santoro and V. Barone, *Phys. Chem. Chem. Phys.*, 2011, **13**, 17007–17012.

[77] Y. Liu, J. Cerezo, F. Santoro, A. Rizzo, N. Lin and X. Zhao, *Phys. Chem. Chem. Phys.*, 2016, **18**, 22889–22905.

[78] J. Cerezo and F. Santoro, *J. Chem. Theory Comput.*, 2016, **12**, 4970–4985.

[79] Y. Liu, L. Martínez-Fernández, J. Cerezo, G. Prampolini, R. Improta and F. Santoro, *Chem. Phys.*, 2018, **515**, 452 – 463.